

# Chapter 1

## Introduction

### 1-1 Introduction of Organic Thin Film Transistors (OTFTs)

The concept of using organic materials as semiconductors layer in transistors are realized at least since the 1980s [1,2]. Recently, the organic thin film transistors (OTFTs) are of interest for the fabrication of low-cost, large-area, flexible displays and low-end electronics. The OTFTs performance has been improved in the past decade and comparable to the hydrogenated amorphous silicon transistors (a-Si:H TFT) [3]. To fabricate organic transistors on glass or flexible substrate, it is essential to lower down the process temperature. Many researchers have proposed individual methods to fabricate the pentacene-transistors and the reported field-effect mobilities are in the range of  $10^{-3} \sim 3\text{cm}^2/\text{V}\cdot\text{sec}$  [4]. However, the OTFTs still face several problems: low-mobility, low-temperature gate dielectrics, and reliably large area processes, etc. Among these issues, a suitable gate dielectric is a major obstacle that must be overcome.

However, the high operating voltage was still a limitation on organic transistors such as the portable applications, especially for RFID requiring low power consumption, it is necessary to reduce the operating voltage to below 7V [5]. A high operating-voltage not only results in high power-consumption, and higher cost on driving circuits; but also damages the organic material. Therefore, to achieve the low-voltage and high performance OTFTs, high-capacitance gate-dielectrics are important demands. Because the accumulated charge density in channel region influenced OTFTs mobility significantly [6]. According to MOSFET theory, the

higher capacitance would accumulate more charge in semiconductor layer under a given gate-voltage. Thus higher capacitance permitted the OTFTs to be operated at lower voltage.

Recently, the high-capacitance gate dielectrics can be achieved by the two methods. One is reducing the gate-dielectric thickness [7], the other was using the high-k material as the gate-dielectrics [8]. However, the high-k materials may arise in high leakage current and low dielectric strength in the utilization of OTFTs. The pinhole may be another question when reducing the dielectric thickness. So, a new dielectric is provided with higher dielectric permittivity, controllable leakage current and tunable thickness. That will be very desirable for OTFTs.

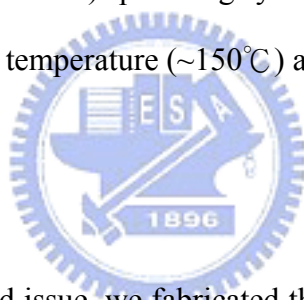
Besides increasing the capacitance, the surface polarity of the gate-dielectric is another concern. Several researchers had verified the hydrophobic surface was more suitable for organic film deposition [9]. Since the hydrophobic polymer dielectric has lower or similar surface energy to organic films. The similar concept was also realized by self-assembled monolayer (SAM) on inorganic dielectrics. If the inorganic dielectrics with lower surface-energy, that may provide better performance and resulted in lower interface traps in OTFTs [10].

However, several reports have discussed the effects of the gate dielectric roughness on OTFTs [11]. The roughness of the gate dielectric can affect the pentacene film deposition and the OTFTs performance.

Finally, if the novel dielectrics with fine surface property and high dielectric quality on which a good organic film could be deposited on, it can overall improve the properties of OTFTs.

## **1-2 Deposition Methods of AlN**

As for III-V compounds, the related researches were focused on the applications of high-power and light-emitting devices [12]. However, the single-crystal compounds can only be grown by metal-organic chemical vapor deposition (MOCVD) or molecular beam epitaxy (MBE) systems...etc [13]. Nevertheless, the high growing temperature and expensive equipment was essentially required. On the other hand, the polycrystalline or amorphous III-V compounds are also utilized in many applications. Low-temperature deposition systems such as sputtering or e-gun evaporation are used to deposit polycrystalline or amorphous III-V compounds [14]. Among the previous systems, the sputtering was chosen for the thin film deposition because of its simplicity and low-temperature processes. In our experiment, with the RF/ICP (Inductively Coupled Plasma) sputtering system, high quality AlN can also be deposited under relatively low temperature ( $\sim 150^{\circ}\text{C}$ ) and room temperature ( $\sim 25^{\circ}\text{C}$ ).



### **1-3 Motivation**

To improve the mentioned issue, we fabricated the OTFT with the AlN film as a new gate dielectric. The AlN film has high chemical stability, high physical stability, and high dielectric permittivity [15]. Moreover, while compared to the oxide-based dielectrics, the wetting property on AlN film was more hydrophobic and the surface free energy was similar to that of the pentacene film.

We also demonstrate two methods to control the gate leakage and the improve of surface roughness in AlN film. Thus, the AlN film shows a low leakage current and a smooth surface.

In this experiment, with the RF sputtering system, the dielectric thickness could be controlled precisely. When reducing the AlN film thickness, the AlN-OTFTs can be operated at low-voltage and exhibit low threshold voltage and extremely low

subthreshold swing.

## **1-4 Thesis Organization**

In Chapter 1, we describe the introduction of OTFTs, deposition methods of AlN, and motivation of the thesis. In Chapter 2, we introduce the transportation mechanisms of organic semiconductor, operation of OTFTs, and parameter extraction. In Chapter 3, the fabrication and the structure of OTFTs are presented. In Chapter 4, electrical properties of AlN dielectric, effects of AlN dielectric roughness, surface polarity of AlN film, low-voltage OTFTs with AlN dielectric, and high-performance AlN-OTFTs are investigated. Finally, we describe the conclusion and future work in Chapter 5.

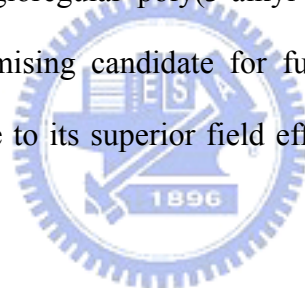


# Chapter 2

## Theoretical Background of OTFTs

### 2-1 Introduction

OTFTs are based on the conjugated polymers, oligoacenes, or fused aromatics. Then, the organic materials can function either as p-type or n-type. In p-type semiconductors, the majority carriers are holes; while in n-type the majority carriers are electrons. Among, p-type semiconductors are the most widely studied organic semiconductors. Recently, many molecular semiconductors, such as pentacene, thiophene oligomers, and regioregular poly(3-alkyl-thiophene) are proposed. The pentacene ( $C_{22}H_{14}$ ) is a promising candidate for future electronic devices and an interesting model system, due to its superior field effect mobility and environmental stability [16].



### 2-2 Transportation Mechanisms of Organic Semiconductor

Carrier transportation in the organic semiconductors have been investigated on the theory and modeling in the past years [17]. Organic conductors are conjugated materials, where the  $\pi$ -electrons are conducted intra the molecular. Its crystalline is formed by relatively weak Van der Waals interaction between molecules, where the molecular-stacking determines the carrier behavior. Thus, the carrier transport were described by different models than the covalent-bonded semiconductors. In covalent-bonded semiconductors, carriers move as highly delocalized plane waves in wide bands and have a very high mobility. But in weak-bonded organic semiconductors, the high-mobility model is no longer valid.

Recently, two principal types of theoretical model are used to describe the transport in organic semiconductors : “The band-transport model” and “The hopping models”. However, band transport may not suit for some disordered organic semiconductors, in which carrier transport is govern by the hopping between localized states. Hopping is assisted by phonons and the mobility increases with temperature. Typically, the mobility is very low, usually much lower than  $1\text{cm}^2/\text{V}\cdot\text{sec}$ . The boundary between “band transport” and “hopping” is divided by materials mobilities ( $\sim 1\text{cm}^2/\text{V}\cdot\text{sec}$ ) at room-temperature (RT) [18]. Many kinds of polycrystalline organic semiconductors , such as several members of the acene series including pentacene, rubrene, have RT mobility over the boundary [19]. Sometimes, temperature-independent mobility was found in some polycrystalline pentacene devices [20]. Thus, this observation argued that the simply thermal activated hopping process governed the whole carrier transport behaviors in high quality polycrystalline pentacene film, despite that the temperature independent mobility has been observed in exceptional cases [20].

The understanding of carrier transport in single crystals of organic semiconductors will help us to understand the transport mechanism in polycrystalline organic semiconductors. The coherent band-like transport of delocalized carriers becomes the prevalent transport-mechanism in the single crystals of organic semiconductors, such as pentacene, tetracene, under the low-temperature environments. The very high hole mobility values have been measured by time-of-flight experiments [21]. Thus, the temperature dependence of the carrier mobility was found below 100K and following with a power law of  $\mu \propto T^{-n}$ ,  $n \sim 1$ , [22], in single crystals of organic semiconductors, consistent with the band-transport model. However, between 100K and 300K, the carrier mobility show a constant value [22], that has been described as the superposition of two independent carrier transport

mechanisms. The first mechanism was small molecular polaron (MP). According to this model the carriers were treated as the heavy; polaron-type; quasi-particles. It is formed by the interaction of the carriers with intra-molecular vibrations of the local lattice environment, and move coherently via tunneling. In this model, the mobility follows the power law  $\mu_{MP}=aT^{-n}$ . The other involves a small lattice polaron (LP), which moves by thermally activated hopping and exhibits a typical exponential dependence of mobility on temperature :  $\mu_{LP}=b\exp[-Ea/kT]$ . The superposition of these two mechanisms could get a good consistence with experimentally measurement of temperature-dependence mobility from room temperature to a Kelvin degrees (K) [23].

Finally, the exact nature of the charge carrier transport in organic molecular crystals is still not well-understood, which has been the focus in many theoretical studies [24].



### 2-3 Operation of OTFTs

Figure 2-1 show two kinds of standard OTFT device configurations, (a) is the top-contact device and (b) is the bottom-contact device, respectively. Actually, the general operation concepts are originated from MOSFET theory. In traditional MOSFET, most devices are operated in inversion mode. However, the operation of OTFTs is generally in accumulation mode [25]. In Fig. 2-2 presents the schematic operation of OTFTs, showing a p-type semiconductor; + indicates a positive charge; - indicates a negative charge. When zero bias was applied to OTFTs, the schematic diagram is shown in Fig. 2-2(a). When a bias,  $V_G$ , is applied to the gate electrode shown in Fig. 2-2(b), (c), the voltage-drop over the insulator and the semiconductor accumulates charges near the insulator/semiconductor interfaces. The typical I-V

characteristics can be used to calculate the important parameters such as mobility, threshold voltage, and on/off current ratio.

Since the pentacene is a p-type semiconductor. Thus, negative bias is applied to the gate, the voltage-drop between insulator and semiconductor cause the band bending in the organic semiconductor. The additional positive charges will accumulate between the interfaces. The energy band diagrams for p-type and n-type OTFT are shown in Fig. 2-3. The insulator serves as a capacitance per unit area which stores charges and can be represented as  $C_{ox}$ , then the accumulated charge per unit area is about  $V_G C_i$ . Additionally, assuming that a negligibly small voltage,  $V_{th}$ , is dropped across the semiconductor. In this situation, the applied drain bias can drive the current from source to drain. The conduction is determined by the mobility ( $\mu$ ) which represents the driving ability of the electrical field on the accumulated charges. Therefore, the increased gate voltage  $\delta V_G$  accounts for the increased charges  $C_{ox} \delta V_G$  and the total charges accumulated over the channel region are  $WLC_{ox} \delta V_G$ , where W and L corresponds to the channel width and length, respectively. If the increment of charge has a mobility:  $\mu$ , and a small drain bias:  $V_D$  is applied then an incremental current  $\delta I_D$  is represented as

$$\delta I_D \approx \frac{W}{L} \mu C_{ox} V_D \delta V_G \quad (2.1)$$

In general, we can divide the operation of OTFTs into two regions, linear and saturation regions. The drain current in the linear region is determined from the following equation:

$$I_D = \frac{W}{L} C_{ox} \mu (V_G - V_{TH} - \frac{V_D}{2}) V_D \quad (2.2)$$

Since the drain voltage is quite small, sometimes equation (2.2) can be simplified as

$$I_D = \frac{W}{L} C_{ox} \mu (V_G - V_{TH}) V_D \quad (2.3)$$

For  $-V_D > -(V_G - V_{TH})$ ,  $I_D$  tends to saturate due to the pinch-off of the



accumulation layer. The current equation is modified as:

$$I_D = \frac{W}{2L} C_{OX} \mu (V_G - V_{TH})^2 \quad (2.4)$$

## 2-4 Parameter Extraction

In this section, the methods of extraction the mobility, the threshold voltage, the on/off current ratio, the subthreshold swing, the maximum interface trap density, and the surface free energy is characterized, respectively.

### 2-4-1 Mobility

Generally, mobility can be extracted from the transconductance maximum  $g_m$  in the linear region:

$$g_m = \left[ \frac{\partial I_D}{\partial V_G} \right]_{V_D = \text{constant}} = \frac{WC_{OX}}{L} \mu V_D \quad (2.5)$$

Mobility can also be extracted from the slope of the curve of the square-root of drain current versus the gate voltage in the saturation region, i.e.  $-V_D > -(V_G - V_{TH})$ :

$$\sqrt{I_D} = \sqrt{\frac{W}{2L} \mu C_{OX} (V_G - V_{TH})} \quad (2.6)$$

### 2-4-2 Threshold voltage

Threshold voltage is related to the operation voltage and the power consumptions of an OTFT. We extract the threshold voltage from equation (2.6), the intersection point of the square-root of drain current versus gate voltage when the device is in the saturation mode operation.

### 2-4-3 On/Off current ratio

Devices with high on/off current ratio represent large turn-on current and small off current. It determines the gray-level switching of the displays. High on/off current ratio means there are enough turn-on current to drive the pixel and sufficiently low off current to keep in low power consumption.

### 2-4-4 Subthreshold swing

Subthreshold swing is also important characteristics for device application. Its is a measure of how rapidly the device switches from the off state to the on state in the region of exponential current increase. Moreover, the subthreshold swing also represents the interface quality and the defect density [26].

$$S = \frac{\partial V_G}{\partial(\log I_D)} \Big|_{V_D = \text{constant}}, \text{ when } V_G < V_T \text{ for p-type.} \quad (2.7)$$

If we want to have good performance TFTs, we need to lower subthreshold swing of transistors.

### 2-4-5 Maximum interface trap density

The maximum number of interface traps density, at the pentacene/dielectric interface can be estimated from the value of the subthreshold swing [26]. Assuming that the densities of deep bulk states and interface states are independent of energy [27]:

$$N_{ss} = \left[ \frac{S \cdot \log(e)}{kT/q} - 1 \right] \cdot \frac{C_i}{q} \quad (2.8)$$

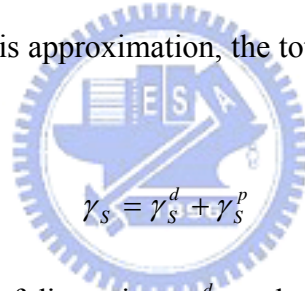
where S is the subthreshold swing,  $C_i$  is the capacitance density, k is Boltzmann's constant, and T is the absolute temperature.

### 2-4-6 Surface free energy

The surface-free-energy of gate dielectrics is a characteristics factor, which affects the performance of the OTFTs. The surface-free-energy was calculated from the contact-angle measurement by using different liquid-drops with different polarities. In our experiments, the Owens, Wendt, Rabel and Kaelble's method (the modified Fowkes' equation) is used to estimate the surface energy [28]:

$$(1 + \cos \theta)\gamma_L = 2(\gamma_s^d \gamma_L^d)^{1/2} + 2(\gamma_s^p \gamma_L^p)^{1/2} \quad (2.9)$$

where  $\theta$  is the contact angle between probing liquid and solid surface;  $\gamma_L$ ,  $\gamma_L^d$  and  $\gamma_L^p$  is the total surface-free-energy, dispersion, and polar component of probing liquid, respectively. From this approximation, the total surface free energy  $\gamma_s$  of the solid surface is:



$$\gamma_s = \gamma_s^d + \gamma_s^p$$

It is characterized by the sum of dispersion  $\gamma_s^d$  and polar  $\gamma_s^p$  components.

### 2-4-7 Poole-Frenkel (P-F) mechanism

The P-F emission is due to the field-enhanced thermal excitation of the trapped electrons in the insulator into the conduction band [29,30]. The current density is given by

$$J = J_0 \exp\left(\frac{\beta_{PF} E^{1/2} - q\phi_{PF}}{k_B T}\right) \quad (2.10)$$

where  $J_0 = \sigma_0 E$  is the low-field current density,  $\sigma_0$  the low-field conductivity,

$\beta_{PF} = (q^3 / \pi \epsilon_0 \epsilon_r)^{1/2}$ , and  $\phi_{PF}$  the height of trap potential well.

# Chapter 3

## Experiments

### 3-1 AlN Deposition

The low temperature AlN films were deposited by a radio frequency inductively coupled plasma (RF-ICP) system [31]. In this system, a 2-inch Al target (purity 99.999%) of the RF gun was immersed in a 4-inch inductive coil which can be controlled by an independent RF coil power. Before the AlN films deposition, the n<sup>+</sup>-Si wafer used as the substrate was rinsed in the deionization water, followed by the initial RCA cleaning. Right before we transferred the wafer into the RF-ICP system, we used acetone with ultrasonic to remove the particles and the impurities and dipped the wafer in the dilute HF solution (HF:H<sub>2</sub>O=1:100) to remove the native oxide on the Si wafer. The system was pumped down to a base pressure less than  $2 \times 10^{-6}$  torr before admitting gas in. A mixed gas of argon and nitrogen was monitored by mass flow controllers at different Ar/N<sub>2</sub> ratio. AlN films were deposited at a total pressure of 2.5mtorr and at a substrate temperature varied from room temperature to 250°C. The RF gun and the inductively coupled coil power can be varied from 0 to 200W and 0 to 180W, respectively. All the relative experiment details were published in our previous reports [31]. The thickness of AlN was estimated by the cross-section image of the scanning electron microscopy (SEM).

### 3-2 OTFTs Fabrication

The devices used in this series of experiments are the top contact (TC) structure,

which means the organic semiconductor layer is deposited on the bottom of the contact electrodes. The detail fabrication processes are following:

#### Step1. Substrate and gate electrode

4-inch n-type heavily-doped single crystal silicon wafer with (100) orientation is used as substrate and gate electrode.

#### Step2. Gate dielectric formation

After the initial acetone cleaning and dilute HF solution, the gate dielectric layer is formed in RF-ICP sputter system. High quality AlN film can be formed under low temperature.



#### Step3. Pentacene film deposition through the shadow mask

The pentacene material obtained from Aldrich without any purification was directly placed in the thermal coater for the deposition. It is well known that the deposition pressure, deposition rate, and deposition temperature are the three critical parameters to the quality of the organic film [32]. The deposition is started at the pressure around  $1 \times 10^{-6}$  torr. The deposition rate is controlled at  $\sim 0.5 \text{ \AA}/\text{sec}$  and the thickness of pentacene film was about 100nm, monitored by the quartz crystal oscillator. Slower deposition rate is expected to result in smoother and better ordering of the organic molecules. The deposition temperature is also a factor influencing the pentacene film formation. The temperature we use in depositing pentacene films is  $70^\circ\text{C}$ . We use shadow mask to define the active region of each device.

Step4. Source/Drain deposition through the shadow mask

The injection barrier of the OTFT device is determined by the materials of the source and drain electrodes. Materials with large work function are preferred to form Ohmic contact [33]. The Au with work function  $\sim 5.1\text{eV}$  does help to provide a better injection. Then, we deposited Au as the source/drain electrodes on the pentacene film. The thickness of the electrode pad is  $1000\text{\AA}$ .

The top contact structure is shown in figure 2-1(a). In this study, all the measured data were obtained from the semiconductor parameter analyzer (HP 4156A) in the darks at room temperature. And we measure the OTFTs immediately when the samples were unloaded from the evaporation chamber.

### 3-3 Capacitance Structure Fabrication

In this study, the structures of metal-insulator-silicon (MIS)-Au/AlN/Si capacitors was fabricated using the following procedure. First, heavily doped n-type silicon (100) substrates were degreased and acid cleaned using an initial RCA cleaning and an HF solution dip. The AlN film was deposited by RF-ICP system. A mixture gas of argon and nitrogen at different Ar/N<sub>2</sub> ratio and the substrates were heated during deposition at different temperature. The top electrode (Au) was defined by shadow mask. The area of the Au pad is  $500\times 500\mu\text{m}^2$ . The Au thickness is about  $700\text{\AA}$ . In the MIS capacitors, AlN films were deposited on blank silicon wafers, and subsequently covered with Au. The MIS structure is shown in figure 3-1.

The MIS was electrically characterized in terms of leakage current and dielectric

constant. Current-voltage (I-V) measurements were done with an HP 4156A parameter analyzer. Capacitance-voltage (C-V) curves were obtained by an HP 4284A C-V meter. The frequency dependence of the capacitances was measured at frequencies from 50Hz to 960KHz.

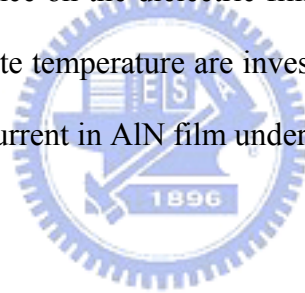


# Chapter 4

## Result and Discussion

### 4-1 Electrical Properties of AlN Dielectric

The high-k gate dielectric generally caused a high leakage current [34]. Therefore, how to suppress the leakage current has become an important subject in the study of transistors [35]. It is known that the processing conditions have an important effect on the properties of high-k materials [36]. During the RF sputtering process, the parameters, such as the substrate temperature, the deposition rate, and the gas flow rate, have a significant influence on the dielectric films. In this study, the effects of nitrogen flow rate and substrate temperature are investigated. Thus, we characterize the permittivity and leakage current in AlN film under different substrate temperatures and Ar/N<sub>2</sub> gas ratio.



#### 4-1-1 Dependence of dielectric leakage on substrate temperature

In past years, many investigations have been carried out concerning the influence of dielectric deposition temperature on the current-voltage characteristics [37,38]. These researchers demonstrated that the dielectric film grown at high deposition temperature shows higher leakage current due to increasing surface roughness.

According to the theory, we tried to control the leakage current by decreasing the substrate temperature during the sputtering process. We deposit three distinct AlN-MIS structure at a Ar/N<sub>2</sub> ratio of 2/9 for the leakage experiment. The AlN film was deposited at the three temperature 250°C, 200°C, and 150°C, respectively. In Fig. 4-1 the change of surface roughness on AlN films could be observed from the



atomic force microscopy (AFM) images with the increase of temperature. The leakage current measured from the MIS structure with 95nm-thick AlN was shown in Fig. 4-2. AlN films deposited under different substrate temperatures are compared. The leakage current densities of the AlN films are about  $1 \times 10^{-9} \text{ A/cm}^2$ ,  $2.4 \times 10^{-9} \text{ A/cm}^2$ ,  $6.2 \times 10^{-9} \text{ A/cm}^2$  at electric field as 1MV/cm for deposition temperatures of 150°C, 200°C, 250°C, respectively. The breakdown fields are more than 5MV/cm, respectively. The AlN deposited at 150°C shows a low leakage current. Whereas the 200°C-AlN and 250°C-AlN dielectrics exhibited larger leakage current, yet these value are acceptable for the device fabrication. These dielectric properties are comparable to those of the thermal SiO<sub>2</sub>, high-k, or polymer gate dielectrics in some reports [8,39,40].

The capacitance-frequency characteristic is also shown in the inset of Fig. 4-2. The frequency dependence of the dielectric capacitances was measured in the range 50Hz to 960KHz. However, under a wide frequency operation range, from 50Hz to 1KHz, the capacitance and the calculated dielectric permittivity are around  $\sim 64 \text{ nf/cm}^2$  and  $\sim 7$ , respectively.

Thus, the result indicates that the leakage current density can be reduced by decreasing the substrate temperature. The leakage current density decreased mainly due to the reduction of surface roughness with decreasing substrate temperature. Because of in the rough surface, the electric field is much stronger than in the smooth surface [41]. The higher electric field can result in higher leakage current. In addition to this, we can also observe that the different substrate temperature of AlN gate dielectric layers with constant capacitance was obtained by adjusting the substrate temperature.

#### 4-1-2 Dependence of dielectric leakage on nitrogen gas flow rate

In past years, some investigations exhibited that repair the vacancies in the dielectric may improve the leakage. As proposed in the metal-oxide dielectrics, the oxygen vacancies were the dominated defects that degraded the dielectric properties. Some researchers introduced the oxygen flow to restore the defects [42]. The dielectric leakage was significantly improved in their results.

According to the theory, we also tried to control the leakage current by increasing the N<sub>2</sub> gas flow rate during the sputtering process. We deposit three distinct AlN-MIS structure at 150°C for the leakage experiment. The AlN film was deposited under different Ar/N<sub>2</sub> gas ratio and each thickness was ~95nm. In Fig. 4-3, it shows that the AFM images of AlN surface roughness from different nitrogen gas flow rate (2/5, 2/7, 2/9). The result indicating that very similar surface roughness was all obtained from different of nitrogen gas flow rate, respectively. As shown in Fig. 4-4, the x-ray photoemission spectrum (XPS) signal from nitrogen ( N 1s) was extracted. When the nitrogen flow rate increased, the nitrogen signal also increased. That implied the nitrogen component could be increased by nitrogen flow rate. The results were also compared as the leakage current density vs. the electric field in Fig. 4-5. As show in the figure, the leakage current increased rapidly in the sample of gas ratio Ar/N<sub>2</sub>: 2/5. When the applied electric field was exceeded 3MV/cm, the leakage current density was more than 10<sup>-4</sup>A/cm<sup>2</sup>. Though there was no significantly dielectric breakdown observed in high electric field. But the leakage resulted in instable and low device yield in our early stage studies. For further reducing the leakage, the Ar/N<sub>2</sub> gas ratio was changed from 2/5 to 2/7 and 2/9. As we could observe, the leakage current was suppressed from 10<sup>-4</sup>A/cm<sup>2</sup> to 10<sup>-9</sup>A/cm<sup>2</sup>. Besides, when the capacitance operated at low electric field (1-2MV/cm), the leakage

current was kept at very low level  $\sim 10^{-10}$  A/cm<sup>2</sup>. The result can come up with other novel low temperature dielectrics [8,43].

To further study the conduction mechanism in AlN, the leakage current-density was plotted as the function of electric field in log-log scale (log(J) vs. log(E)) in Fig. 4-6(a). Clearly, two transports in AlN film were observed. A good Ohmic-conduction could be fitted under low electric field, but the conduction transferred into nonlinear under high electric field. If the Ar/N<sub>2</sub> gas ratios was changed from 2/5 to 2/7 and 2/9, the transfer point of the electric filed was also changed from 0.8 to 1.2 and 2.7MV/cm, respectively. Thus, the J-E curves was plotted as Poole-Frenkel plots (ln(J/E) vs. E<sup>1/2</sup>) in Fig. 4-6(b). The slope ( $\beta/k_B T$ ) of the straight line in Fig. 4-6(b) is:

$$\beta/k_B T = \sqrt{\frac{q^3}{\pi \epsilon_0 \epsilon_r}}$$

where  $q$  is the electron charge,  $k_B$  is the Boltzmann's constant,  $T$  is the absolute temperature,  $\epsilon_0$  is the absolute dielectric constant,  $\epsilon_r$  is the relative dielectric constant. By fitting the slope ( $\beta/k_B T$ ) in Fig. 4-6(b), the slope is 11.2, 11, 10.9 (cm/MV)<sup>1/2</sup> at the Ar/N<sub>2</sub> ratio: 2/5, 2/7, 2/9, respectively. The relative dielectric constant determined from the slope is 6.8, 7.1, 7.2, respectively. From the capacitance measurement of the impedance analyzer (HP 4284A), the estimated dielectric constant was about 6.28, 6.82, 7.32 at Ar/N<sub>2</sub> ratio: 2/5, 2/7, 2/9, respectively. They yield the various values of the dielectric constant and the constant  $\beta_{PF}/k_B T$ , as shown in Table I. It was good agree with the proposed Poole-Frenkel transport in AlN. If we consider the defect distribution in AlN film, it is investigated that the corresponding defects near the conduction band were the nitrogen vacancies [44,45]. Thus, the increase of nitrogen flow rate in the sputtering process may be an affective way to compensate the nitrogen vacancies and suppress the potential leakage path in

AlN.

Thus, the result indicates that the leakage current density can be reduced by increasing the nitrogen gas flow rate. Therefore, according to the hypothesis, by compensating the none-metallic element in the compound dielectric should be a practicable method for reducing leakage. The dielectric leakage was significantly improved.

In the short summary, the leakage current density decreased can be improved by increasing nitrogen flow rate and decreasing substrate temperature.

#### **4-2 Effects of AlN Dielectric Roughness**

Current research on gate dielectric is improving the performance of organic thin film transistors (OTFTs). It is generally accepted that the surface roughness of the gate dielectric is an important parameter that affects the electrical performance of OTFTs [11,46]. In recent work, rougher gate dielectrics have been shown to result in smaller grains and lower the mobility in OTFTs. According to the result, we might try to deduce the AlN surface roughness.

In the experiments, we compare the morphology of pentacene and devices characteristics to the different roughness of AlN gate dielectrics. The devices structure and the fabrication procedure were described in section 3-2.

Firstly, by changing the deposition temperature of the AlN gate dielectric, the surface morphologies were obtained from their atomic force microscopy (AFM) images, as shown in figures 4-7 (a) (b) and (c). Clearly, the average surface roughness decreased from 0.43, 0.31, to 0.17nm while the deposition temperature was varied from 250°C, 200°C, to 150°C and at a Ar/N<sub>2</sub> ratio: 2/9. It is also known that the dielectric surface roughness has a strong influence on the pentacene deposition

[11,47]. In figures 4-7 (d) (e) and (f), we compare the morphology of pentacene film grown on these three of AlN films, correspondingly. As the AlN surface becomes smoother, the grown pentacene film turns to be dendritic structure and exhibits larger grain size.

In order to determine the influence of roughness on OTFTs, the electrical properties of OTFTs from different gate dielectric roughness were characterized. The transfer characteristics of the OTFTs with AlN dielectrics grown at different temperatures and at a Ar/N<sub>2</sub> ratio: 2/9 are shown in Fig. 4-8. The drain voltage is biased as -3V to keep the devices operated under linear region. The gate voltage was scanned from +2V to -10V. When the AlN deposition temperature is varied from 250°C, 200°C, to 150°C, the device subthreshold swing is improved from 0.6V/decade to 0.4V/decade and the device output current is enlarged more than one order. Since the subthreshold swing represents the interface quality and the defect density, we calculate the maximum interface trap density by equation (2.8).

$$N_{ss} = \left[ \frac{S \cdot \log(e)}{kT/q} - 1 \right] \cdot \frac{C_i}{q}$$

By assuming  $C_i = 64 \text{ nf/cm}^2$  and  $S = 0.4, 0.5, 0.6 \text{ V/decade}$ , respectively. The approximate interface trap density in our devices is  $2.28 \times 10^{12}$ ,  $2.95 \times 10^{12}$ , and  $3.62 \times 10^{12} \text{ cm}^{-2} \text{ eV}^{-1}$ , respectively. This result is comparable to other dielectrics in OTFTs [10,26,39,48].

Additionally, lowering the AlN temperature also reduces the device threshold voltage. The Fig. 4-9 depicts the curves of  $\sqrt{I_D}$  vs.  $V_G$ , the x-axis interval reveals that OTFTs with 250°C AlN film have higher threshold voltage as -6V while those with 200°C and 150°C AlN films have lower threshold voltage as -2V. The output characteristics of the proposed OTFTs with AlN-dielectric grown at different temperatures are also shown in Fig. 4-10, Fig. 4-11, Fig. 4-12, respectively.

The improvement of the device performance by reducing the AlN deposition temperature can be further studied by comparing their field effect mobility in Fig. 4-13. The mobility is extracted from the linear region transconductance as equation (2.5).

$$\mu = \frac{L}{V_D WC_i} \left. \frac{\partial I_D}{\partial V_G} \right|_{V_D = \text{const}}$$

It is compared that the mobility of devices with 150°C AlN film, 200°C AlN film, and 250°C AlN film, the former two have larger maximum mobility such as 0.24 cm<sup>2</sup>/V-sec for 150°C AlN-OTFT and 0.04cm<sup>2</sup>/V-sec for 200°C AlN-OTFT. Those devices with AlN deposited at 250°C, however, exhibit much lower maximum mobility around 10<sup>-3</sup>cm<sup>2</sup>/V-sec. It is also observed that the field effect mobility of devices with 250°C AlN film suffers pronounce degradation under high gate bias due to surface irregular causes locally strong electric field and results in leakage and also increases the surface scattering effect.

In the short summary, it can be concluded that lowering the AlN deposition temperature gives smoother surface and larger pentacene grain size. The field effect mobility is also accordingly improved.

### 4-3 Surface Polarity of AlN Film

In general, the pentacene deposition and the OTFTs performance are strongly influenced by the organic/dielectric interaction. To enhance the performance, the surface polarity was one of the key issues. Recently, researchers showed interface defects can be minimized by altering dielectric polarity such as SAM-treatment or the polymer dielectric [9,10,49]. Base on the suggestion, we might try to investigate the AlN surface polarity.

In this experiment, we used de-ionized water and glycerol as the polar liquid pair, and di-iodomethane was chosen as the none-polar liquid. According to our measurement, the contact angle between AlN-D.I. water, AlN-glycerol, AlN-diiodomethane was  $77.0^{\circ}\pm 2^{\circ}$ ,  $56.1^{\circ}\pm 1^{\circ}$ ,  $40.4^{\circ}\pm 4^{\circ}$ . By equation (2.9)

$$(1 + \cos \theta)\gamma_L = 2(\gamma_S^d \gamma_L^d)^{1/2} + 2(\gamma_S^p \gamma_L^p)^{1/2}$$

, the total surface free energy of AlN was  $38.5\pm 1$  (mJ/m<sup>2</sup>). As summarized in Table II, the AlN had low surface energy. The results indicate that the surface in AlN gate dielectric was hydrophobic and had a low polarity. To our surprise, the surface free energy was lower than polymer dielectrics, pentacene, and the HMDs treated SiO<sub>2</sub>. It was almost close to the OTS-treated SiO<sub>2</sub> [49,50,51]. The particular characteristic is contrary to the other ceramic-based dielectrics. The similar affinity between pentacene and dielectrics may be helpful for reducing traps when depositing organic film on dielectrics [52]. That may be a reasonable explaining for AlN-OTFTs having the outstanding sub-threshold swing and low interface trap density.

In the short summary, we have demonstrated that the surface of AlN gate dielectric was very hydrophobic and lowly polar. Thus, this result indicates that the AlN gate dielectric with well-defined surface property and more compatible the growth of pentacene.

#### **4-4 Low-Voltage OTFTs with AlN Dielectric**

Recently, one of the key problems with existing organic TFTs is their large operating voltage, which often exceeds 20V. Thus, to further decrease the operating voltage, increasing the dielectric capacitance is effectively [7,8,53]. Base on the method, we might try to increase the AlN dielectric capacitance. In this experiment, the thickness of AlN dielectric would be reduced to achieve a high capacitance to

operate OTFTs at a low voltage.

According to previous sections, it is known that the 150°C AlN film with Ar/N<sub>2</sub> gas ratio about 2/9 showed the potential for reducing the thickness to increase the OTFTs capacitance. Thus, for further improving the operating voltage of AlN-OTFTs, we used the thinner AlN film as the gate dielectric. It is confirmed that the thickness of AlN film from scanning electron microscopy (SEM) in Fig. 4-14. The thickness of AlN film was about 60nm.

From the MIS structure, the capacitances were measured at the frequency of 50Hz to 960KHz in the inset of Fig. 4-15. The corresponding capacitance was about 93nf/cm<sup>2</sup> from 50Hz to 1KHz. The gate leakage was characterized in Fig. 4-15, the leakage was as low as  $\sim 10^{-8}$ A/cm<sup>2</sup> under electric field at 1MV/cm. The plot of Log I<sub>D</sub> vs. V<sub>G</sub> and  $\sqrt{I_D}$  vs. V<sub>G</sub> was shown in Fig. 4-16(a) and 4-16(b), respectively. In Fig. 4-16(a), the AlN-OTFT was operated less than 5V. The high on/off current ratio more than 5 was also achieved even under extremely low drain bias -0.5V. Additionally, the subthreshold swing can be as low as  $\sim 0.13$ V/decade at a drain voltage of -3V. From Fig. 4-16(b), the extracted threshold voltage and the field effect mobility in saturation region was about -1.5V and 0.02cm<sup>2</sup>/V-sec, respectively. On the other hand, the output characteristics were shown in Fig. 4-17, the transistor could be easily operated in saturation region at low drain voltage about -3V. For further investigating, we may focus on the interface quality of semiconductor (pentacene) and insulator (AlN) from the AlN-OTFTs performance. Since the maximum interface trap density could be estimated by the previous equation. By assuming C<sub>i</sub>  $\sim 93$ nf/cm<sup>2</sup> and S = 0.13V/decade. From our calculation, the approximated interface trap density in our devices is  $6.8 \times 10^{11}$ cm<sup>-2</sup>eV<sup>-1</sup>. This trap density was quite low and comparable with other dielectrics in OTFTs [10,26,39,48].



In the short summary, the key to low-voltage operation is the reduction of dielectric thickness. The high capacitance of the thin AlN dielectric make the OTFTs to operate at a relative low voltage about 5V and exhibit low threshold voltage and a extremely low subthreshold swing. Thus, the AlN-OTFTs showed the potential application as low-voltage and rapid switched organic transistors.

#### **4-5 High-Performance AlN-OTFTs**

In recent years, organic thin film transistors (OTFTs) exhibit great potential for mass production of active-matrix displays and organic electronics. In the future, the OTFTs will be fabricated on clothes or paper substrate for flexible application and battery-powered device application [5,54]. Thus, to develop an low-voltage OTFTs at low process temperature (below 100°C ) is very desirable.

According to above sections, the author demonstrated the control of gate leakage of AlN film. As the result of these optimized parameters, thus, in this experiment, we tried to fabricate thin AlN film as the gate insulator at higher Ar/N<sub>2</sub> ratio and/or at room temperature(~25°C).

##### **4-5-1 AlN dielectric with higher Ar/N<sub>2</sub> ratio**

We deposited AlN at a higher Ar/N<sub>2</sub> ratio: 2/12 and at a substrate temperature 150°C. In Fig. 4-18, we showed the AFM image of AlN film. The AlN film was smooth at higher Ar/N<sub>2</sub> ratio. The surface roughness was only about 0.18nm. In Fig. 4-19, shows the pentacene grains on the AlN insulator. The pentacene films exhibited a large grain size, too. Actually, the roughness degradation and pinhole may arise when reducing the dielectric thickness. In the higher Ar/N<sub>2</sub> ratio

sputtered-AlN film, no significant surface irregular and pinholes were appeared in our observation. Additionally, the higher Ar/N<sub>2</sub> ratio AlN film showed good dielectric properties. From the MIS structure, the capacitances were measure at the frequency of 50Hz to 960KHz in the inset of Fig. 4-20. The capacitance was about 104nf/cm<sup>2</sup> from 50Hz to 1KHz. The gate leakage was characterized in Fig. 4-20, the leakage was about 9.8×10<sup>-9</sup>A/cm<sup>2</sup> under electric field at 1MV/cm.

Subsequently, we exhibited the transistor characteristics. The channel width and length were defined as 600μm and 100μm. The AlN-OTFT was fabricated on the extremely thin AlN film. From the SEM image in Fig. 4-21, we estimate the thickness of AlN film is about 50nm. The transfer characteristic was showed in Fig. 4-22. The AlN-OTFTs could be operated at relative low voltage (~5V), the on/off current ratio was also remained highly (~10<sup>5</sup>). The field effect mobility in the linear region were 1.29cm<sup>2</sup>/V-sec, and 1.41cm<sup>2</sup>/V-sec at drain bias were -0.5, and -1V, respectively. In Fig. 4-23, shows the plot of (I<sub>D</sub>)<sup>1/2</sup> vs. V<sub>G</sub> at a drain voltage of -3V. The threshold voltage was only -2.1V and the field effect mobility in saturation region was about 1.67cm<sup>2</sup>/V-sec. The subthreshold swing was 350mV/decade at a drain voltage of -3V. The mobility of ~1.67cm<sup>2</sup>/V-sec was close to the averaged best records for OTFTs [39]. Output characteristics were also showed in Fig. 4-24, the AlN-OTFTs could be operated in saturation region at low drain bias (~3V). Since the subthreshold swing represents the interface quality and the traps behavior [26], we may calculate the maximum interface trap density by previous equation. By assuming C<sub>i</sub>=104nf/cm<sup>2</sup> and S = 350mV/decade, the approximate interface trap density in our devices is 3.16×10<sup>12</sup>cm<sup>-2</sup>eV<sup>-1</sup>.

#### 4-5-2 Room temperature AlN dielectric

In early stage, we deposited the AlN film at higher substrate temperature. The AlN film has grains and is highly c-axial oriented [31]. As for gate dielectrics, grain boundaries could influence the surface roughness and reduce the uniformity. Generally, the grain boundaries may also serve as leakage paths. Since the dielectric roughness and leakage are essential demands for OTFTs fabrication. In this experiments, we deposited AlN at lower substrate temperature and at a Ar/N<sub>2</sub> ratio: 2/9. In Fig. 4-25, we showed the AFM image of room temperature AlN film. In contrary to our former results, the room temperature AlN film was smooth. The surface roughness was only about 0.2nm. In Fig. 4-26 shows the pentacene grains on the AlN insulator. The pentacene films exhibited a large grain size. Actually, the roughness degradation and pinhole may arise when reducing the dielectric thickness. In the room temperature sputtered-AlN film, no significant surface irregular and pinholes were appeared in our observation. Additionally, the room temperature AlN film showed good dielectric properties. From the MIS structure, the capacitances were measure at the frequency of 50Hz to 960KHz in the inset of Fig. 4-27. The capacitance was about 104nf/cm<sup>2</sup> from 50Hz to 1KHz. The gate leakage was characterized in Fig. 4-27, the leakage was about  $9.5 \times 10^{-9}$  A/cm<sup>2</sup> under electric field at 1MV/cm.

Subsequently, we exhibited the transistor characteristics. The channel width and length were defined as 600 $\mu$ m and 50 $\mu$ m. The AlN-OTFT was fabricated on the extremely thin AlN film. From the SEM image in Fig. 4-28, we estimate the thickness of AlN film is about 50nm. The transfer characteristic was showed in Fig. 4-29. The AlN-OTFTs could be operated at relative low voltage ( $\sim$ 5V), the on/off current ratio was also remained highly ( $>10^6$ ). The field effect mobility in the linear region was 0.16cm<sup>2</sup>/V-sec, and 0.14cm<sup>2</sup>/V-sec at drain bias -0.5V, and -1V, respectively. In Fig. 4-30 shows the plot of ( $I_D$ )<sup>1/2</sup> vs.  $V_G$  at a drain voltage of -3V.

The threshold voltage was only -1.8V and the field effect mobility in saturation region was about  $0.082\text{cm}^2/\text{V}\cdot\text{sec}$ . The promising subthreshold swing was only 190 mV/decade at a drain voltage of -3V. The magnitude was almost approximately the theoretical minimum  $\sim 58\text{mV}/\text{decade}$  ( $kT/q \cdot \ln(10)$ ) [55]. Output characteristics were also showed in Fig. 4-31, the AlN-OTFTs could be operated in saturation region at low drain bias ( $\sim 3\text{V}$ ). Since the subthreshold swing represents the interface quality and the traps behavior [26], we may calculate the maximum interface trap density by equation (2.8). By assuming  $C_i=104\text{nf}/\text{cm}^2$  and  $S = 190\text{mV}/\text{decade}$ , the approximate interface trap density in our devices is  $1.4 \times 10^{12}\text{cm}^{-2}\text{eV}^{-1}$ . The trap density was almost close to the lowest trap density reported for organic transistors.

#### 4-6 Summary

The pentacene-based OTFTs with low temperature ( $\sim 25^\circ\text{C}$ ) and high Ar/N<sub>2</sub> ratio (2/12) AlN gate insulator had been fabricated and characterized. With the combination of favorable properties, demonstrates that OTFTs successfully at voltages about 5V and exhibited very high field effect mobility.

# Chapter 5

## Conclusion and Future Work

### 5-1 Conclusion

A new low-temperature gate-dielectric, AlN film, is proposed for OTFTs. The pinhole free, smooth and extremely thin AlN film can be deposited by the RF-sputtering system at low deposition temperature (from 150°C to 25°C). The dielectric leakage was significantly low, and the AlN has a surface free energy that is similar to that of the pentacene film. It can be concluded that lowering the AlN deposition temperature gives smaller leakage current and larger pentacene grain size. The field effect mobility is accordingly improved. The process is promising for the development of low-temperature OTFTs. The Ar/N<sub>2</sub> flow ratio in the sputtering process was demonstrated to be a key parameter in reducing AlN gate leakage. Poole-Frenkel-related leakage is suppressed as the electric field increased.

Based on experimental result, the low-voltage and high performance OTFTs are realized. With the thinner AlN gate-dielectric, lower substrate temperature, and higher Ar/N<sub>2</sub> ratio, the AlN-OTFTs can be operated at low-voltage (about 5V). From the series of the experiments, the highest field effect mobility is 1.67cm<sup>2</sup>/V-sec, the lowest subthreshold swing is 130mV/decade, and the lowest threshold voltage -1.5V, respectively. The high on/off current ratio about 10<sup>6</sup> were all observed from these AlN-OTFTs. According to the mentioned electric properties, it is demonstrated that the AlN-OTFT has potential application in low-voltage and rapid-switching organic transistors.

## 5-2 Future Work

Since the AlN-OTFTs on silicon substrate was successfully fabricated. Further studies will focus on realizing the AlN-OTFTs on glass and on flexible substrates. The leakage mechanism needs more detail experimental result to verify the influence of nitrogen-related defect. The growth of pentacene film on AlN is still a un-discovered evidence. The growing mechanism should be a interesting study. However, the improvement is also expected by pentacene purification and S/D resistance reduction in future studies.



## References

- [1] A. Tsumura, K. Koezuka, and T. Ando, "Macromolecular electronic devices: Field-effect transistor with a polythiophene thin film", *Appl. Phys. Lett.* vol.49, pp. 1210, (1986).
- [2] J. H. Burroughes, C. A. Jones, and R. H. Friend, "Polymer diodes and transistors: new semiconductor device physics", *Nature*, vol. 335, pp.137, (1988).
- [3] Y. Y. Lin, D. J. Gundlach, S. F. Nelson, and T. N. Jackson, "Pentacene organic thin-film transistors-molecular ordering and mobility", *IEEE Electron Device Lett.* vol. 18, pp. 87, (1997).
- [4] C. D. Dimitrakopoulos and P. R. L. Malenfant, "Organic thin film transistors for large area electronics", *Adv. Mater. (Weinheim, Ger.)* 14, No. 2, pp.99, (2002).
- [5] H. Klauk, M. Halik, U. Zschieschang, F. Eder, D. Rohde, G. Schmid, and C. Dehm, "Flexible organic complementary circuits", *IEEE Trans. Electron Devices*, vol. 52, pp. 618, (2005).
- [6] C. D. Dimitrakopoulos, S. Purushothaman, J. Kymissis, A. Callefari, J. M. Shaw, "Low-voltage organic transistors on plastic comprising high-dielectric-constant gate insulator", *Science*, vol. 283, pp. 822, (1999).
- [7] Sang Yoon Yang, Se Hyun Kim, Kwonwoo Shin, Hayoung Jeon, and Chan Eon Park, "Low-voltage pentacene field-effect transistors with ultrathin polymer gate dielectrics", *Appl. Phys. Lett.*, vol. 88, pp. 173507, (2006).
- [8] Guangming Wang, Daniel Moses, Alan J. Heeger, Hong-Mei Zhang, Mux Narasimhan, and R. E. Demaray, "Poly(3-hexylthiophene) field-effect transistors with high dielectric constant gate insulator", *J. Appl. Phys.*, vol. 95, pp. 316, (2004).

- [9] G. Nunes Jr., S. G. Zane, and J. S. Meth, "Styrenic polymers as gate dielectrics for pentacene field-effect transistors", *J. Appl. Phys.*, vol. 98, pp. 104503, (2005).
- [10] M. McDowell, I. G. Hill, J. E. McDermott, S. L. Bernasek, and J. Schwartz, "Improved organic thin-film transistor performance using novel self-assembled monolayers", *Appl. Phys. Lett.*, vol. 88, pp. 073505, (2006).
- [11] Sandra. E. Fritz, Tommie Wilson Kelley, and C. Daniel Frisbie, "Effect of Dielectric Roughness on Performance of Pentacene TFTs and Restoration of Performance with a Polymeric Smoothing Layer", *J. Phys. Chem. B*, vol.109, pp.10574, (2005).
- [12] H. Harima, T. Inoue, S. Nakashima, H. Okumura, Y. Ishida, S. Yoshida, T. Koizumi, H. Grille, and F. Bechstedt, "Raman studies on phonon modes in cubic AlGaN alloy", *Appl. Phys. Lett.*, vol. 74, pp. 191, (1999).
- [13] L. Chen, B. J. Skromme, R. F. Dalmau, R. Schlessler, Z. Sitar C. Chen, W. Sun, J. Yang, M. A. Khan, M. L. Nakarmi, J. Y. Lin, and H.-X. Jiang, "Band-edge exciton states in AlN single crystals and epitaxial layers", *Appl. Phys. Lett.*, vol. 85, pp. 4334, (2004).
- [14] K. K. Harris, B. P. Gila, J. Deroaches, K. N. Lee, J. D. MacKenzie, C. R. Abernathy, F. Ren, and S. J. Pearton, "Microstructure and Thermal Stability of Aluminum Nitride Thin Films Deposited at Low Temperature on Silicon", *J. Electrochem. Soc.*, vol. 149, pp. G128, (2002).
- [15] Laurie Valbin, Laure Sevely, and Serge Spirkovitch, "Low temperature piezoelectric aluminum nitride thin film", *Proceeding of SPIE*, vol. 4174, pp.154, (2000).
- [16] Yanming Sun, Yunqi Liu, and Daoben Zhu, "Advances in organic field-effect transistors", *J. Mater. Chem.*, vol. 15, pp. 53, (2005).
- [17] R. A. Street, D. Knipp, and A. R. Völkel, "Hole transport in polycrystalline



- pentacene transistors”, *Appl. Phys. Lett.*, vol. 80, pp. 1658, (2002).
- [18] G. Horowitz, “Organic field-effect transistors”, *Adv. Mater.*, vol. 10, pp. 365, (1998).
- [19] Y.-Y. Lin, D. J. Gundlach, S. F. Nelson, and T. N. Jackson, “Stacked pentacene layer organic thin-film transistors with improved characteristics”, *IEEE Electron Device Lett*, vol. 18, pp 606, (2000).
- [20] S. F. Nelson, Y.-Y. Lin, D. J. Gundlach, and T. N. Jackson, “Temperature-independent transport in high-mobility pentacene transistors”, *Appl. Phys. Lett.*, vol. 72, pp. 1854, (1998).
- [21] W. Warta, and N. Karl, “Hot holes in naphthalene: High, electric-field-dependent mobilities”, *Phys. Rev. B*, vol. 32, pp. 1172, (1985).
- [22] L. B. Schein, C. B. Duke, and A. R. McGhie, “Observation of the Band-Hopping Transition for Electrons in Naphthalene”, *Phys. Rev. Lett.*, vol 40, pp. 197, (1978).
- [23] E. A. Silinsh, A. Klimkans, S. Larsson, and V. Capek, “Molecular polaron states in polyacene crystals. Formation and transfer processes”, *Chem. Phys.*, vol 198, pp. 311 (1995).
- [24] O. Ostroverkhova, D. G. Cooke, S. Shcherbyna, R. F. Egerton, F. A. Hegmann, R. R. Tykwinski, and J. E. Anthony, “Bandlike transport in pentacene and functionalized pentacene thin films revealed by subpicosecond transient photoconductivity measurements”, *Phys. Rev. B*, vol. 71, pp. 035204, (2005).
- [25] A. R. Brown, C. P. Jarrett, D. M. de Leeuw, and M. Matters, “Field-effect transistors made from solution-processed organic semiconductors”, *Synth. Met.*, vol. 88, pp. 37, (1997).
- [26] K N Narayanan Unni, Sylvie Dabos-Seignon, and Jean-Michel Nunzi, “Improved performance of pentacene field-effect transistors using a polyimide gate

- dielectric layer”, J. Phys. D: Appl. Phys., vol. 38, pp. 1148, (2005).
- [27] A. Rolland, J. Richard, J. P. Kleider, and D. Mencaraglia, “Electrical properties of amorphous silicon transistors and MIS-devices: Comparative study of top nitride and bottom nitride configurations”, J. Electrochem. Soc., vol. 140, pp. 3679, (1993).
- [28] Kui-Xiang Ma, Chee-Hin Ho, Furong Zhu, and Tai-Shung Chung. “Investigation of surface energy for organic light emitting polymers and indium tin oxide”, Thin Solid Films, vol. 371, pp. 140, (2000).
- [29] S. M. Sze, Physics of Semiconductor Devices, Chap. 7, pp. 402, Wiley, New York, (1981).
- [30] Po-Tsun Liu, Ting-Chang Chang, Ya-Liang Yang, Yi-Fang Cheng, Jae-Kyun Lee, Fu-Yung Shih, Eric Tsai, Grace Chen, and Simon M. Sze, “Improvement on intrinsic electrical properties of low- $k$  hydrogen silsesquioxane/copper interconnects employing deuterium plasma treatment”, J. Electrochem. Soc., vol. 147, pp. 1186, (2000).
- [31] C.-M. Yeh, C.H. Chen, J.-Y. Gan, C.S. Kou, and J. Hwang, “Enhancement of the c-axis texture of aluminum nitride by an inductively coupled plasma reactive sputtering process”, Thin Solid Films, vol. 483, pp. 6, (2005).
- [32] C. D. Dimitrakopoulos, A. R. Brown, and A. Pomp, “Molecular beam deposited thin films of pentacene for organic field effect transistor applications”, J. Appl. Phys., vol. 80, pp. 2501, (1996).
- [33] Chih-Wei Chu, Sheng-Han Li, Chieh-Wei Chen, Vishal Shrotriya, and Yang Yang, “High-performance organic thin-film transistors with metal oxide/metal bilayer electrode”, Appl. Phys. Lett., vol. 87, pp. 193508, (2005).
- [34] R. W. I. de Boer, N. N. Iosad, A. F. Stassen, T. M. Klapwijk, and A. F. Morpurgo, “Influence of the gate leakage current on the stability of organic single-crystal

- field-effect transistors”, *Appl. Phys. Lett.*, vol. 86, pp. 032103, (2005).
- [35] Jun Wang, Xuanjun Yan, Yanxia Xu, Jian Zhang, and Donghang Yan, “Organic thin-film transistors having inorganic/organic double gate insulators”, *Appl. Phys. Lett.*, vol. 85, pp. 5424, (2004).
- [36] Wenfeng Xiang, Huibin Lü, Lei Yan, Haizhong Guo, Lifeng Liu, Yueliang Zhou, Guozhen Yang, Jinchun Jiang, Huansheng Cheng, and Zhenghao Chen, “Characteristics of  $\text{LaAlO}_3/\text{Si}(100)$  deposited under various oxygen pressures”, *J. Appl. Phys.*, vol. 93, pp. 533, (2003).
- [37] Yi-Hsien Lee, Jenn-Ming Wu, Yu-Lun Chueh, and Li-Jen Chou, “Low-temperature growth and interface characterization of  $\text{BiFeO}_3$  thin films with reduced leakage current”, *Appl. Phys. Lett.*, vol. 87, pp. 172901, (2005).
- [38] Yun-Hi Lee, Young-Sik Kim, Byeong-Kwon Ju, and Myung-Hwan Oh, “Roughness of  $\text{ZnS:Pr,Ce/Ta}_2\text{O}_5$  interface and its effects on electrical performance of alternating current thin-film electroluminescent devices”, *IEEE Trans. Electron Devices*, vol. 46, pp. 892, (1999).
- [39] H. Klauk, M. Halik, U. Zschieschang, G. Schmid, W. Radlik, and W. Weber, “High-mobility polymer gate dielectric pentacene thin film transistors”, *J. Appl. Phys.*, vol. 92, pp.5259, (2002).
- [40] Keiji Ueno, Shigeomi Abe, Ryo Onoki, and Koichiro Saiki, “Anodization of electrolytically polished Ta surface for enhancement of carrier injection into organic field-effect transistors,” *J. Apply. Phys.*, vol.98, pp.114503-1, (2005).
- [41] Y. S. Kim, M. Y. Sung, Y. H. Lee, B. K. Ju, and M. H. Oh, “The influence of surface roughness on the electric conduction process in amorphous  $\text{Ta}_2\text{O}_5$  thin films”, *J. Electrochem. Soc.*, vol. 146, pp. 3398, (1999).
- [42] Chang Su Kim, Woo Jin Kim, Sung Jin Jo, Sung Won Lee, Se Jong Lee, and Hong Koo Baik, “Influence of the oxygen concentration of YSZ gate dielectric

- layer on the low voltage operating pentacene thin film transistor”, *Electrochem. Solid-State Lett.*, vol. 9, pp. G96, (2006).
- [43] KyongTae Kang, Mi-Hwa Lim, Ho-Gi Kim, YongWoo Choi, Harry L. Tuller, Il-Doo Kim, and Jae-Min Hong, “Mn-doped  $Ba_{0.6}Sr_{0.4}TiO_3$  high- $K$  gate dielectrics for low voltage organic transistor on polymer substrate”, *Apply. Phys. Lett.*, vol. 87, pp. 242908, (2005).
- [44] X. Li, T. L. Tansley and V. W. L. Chin, “Dielectric properties of AlN films prepared by laser-induced chemical vapour deposition”, *Thin Solid Films*, vol. 250, pp. 263, (1994).
- [45] T. L. Tansley and R. J. Egan, “Point-defect energies in the nitrides of aluminum, gallium, and indium”, *Phys. Rev. B*, vol. 45, pp. 10942, (1992).
- [46] Kwonwoo Shin, Chanwoo Yang, Sang Yoon Yang, Hayoung Jeon, and Chan Eon Park, “Effects of polymer gate dielectrics roughness on pentacene field-effect transistors”, *Appl. Phys. Lett.*, vol. 88, pp. 072109, (2006).
- [47] Hagen Klauk, David J. Gundlach, Jonathan A. Nichols and Thomas N. Jackson, ”Pentacene Organic Thin-Film Transistors for Circuit and Display Applications”, *IEEE Trans. Electron Device*, vol. 46, pp. 1258, (1999).
- [48] D. Knipp, R. A. Street, A. Volkel, and J. Ho, “Pentacene thin film transistors on inorganic dielectrics: Morphology, structural properties, and electronic transport”, *J. Apply. Phys.*, vol. 93, pp. 347, (2003).
- [49] Sang Chul Lim, Seong Hyun Kim, Jung Hun Lee, Mi Kyung Kim, Do Jin Kim, and Taehyoung Zyung, “Surface-treatment effects on organic thin-film transistors”, *Synth. Met.*, vol. 148, pp. 75, (2005).
- [50] Yunseok Jang, Do Hwan Kim, Yeong Don Park, Jeong Ho Cho, Minkyu Hwang, and Kilwon Cho, “Influence of the dielectric constant of a polyvinyl phenol insulator on the field-effect mobility of a pentacene-based thin-film transistor”,

- Appl. Phys. Lett., vol. 87, pp. 152105, (2005).
- [51] M. Yoshida, S. Uemura, T. Kodzasa, T. Kamata, M. Matsuzawa, and T. Kawai, “Surface potential control of an insulator layer for the high performance organic FET”, Synth. Met., vol. 137, pp. 967, (2003).
- [52] Sang Yoon Kwonwoo, Kwonwoo Shin, and Chan Eon Park, “The Effect of Gate-Dielectric Surface Energy on Pentacene Morphology and Organic Field-Effect Transistor Characteristics”, Adv. Funct. Mater., vol. 15, pp. 1806, (2005).
- [53] L. A. Majewski, R. Schroeder, and M. Grell, “Low-voltage, high-performance organic field-effect transistors with an ultra-thin TiO<sub>2</sub> layer as gate insulator”, Adv. Funct. Mater., vol. 15, pp. 1017, (2005).
- [54] Florian Eder, Hagen Klauk, Marcus Halik, Ute Zschieschang, Günter Schmid, and Christine Dehm, “Organic electronics on paper”, Appl. Phys. Lett., vol. 84, pp. 2673, (2004).
- [55] Christopher R. Newman, C. Daniel Frisbie, Demetrio A. da Silva Filho, Jean-Luc Bredas, Paul C. Ewbank, and Kent R. Mann, “Introduction to organic thin film transistors and design of n-channel organic semiconductors”, Chem. Mater., vol. 16, pp. 4436, (2004).
- [56] Yunseok Jang, Do Hwan Kim, Yeong Don Park, Jeong Ho Cho, Minkyu Hwang, and Kilwon Cho, “Low-voltage and high-field-effect mobility organic transistors with a polymer insulator”, Appl. Phys. Lett., vol. 88, pp. 072101, (2006).
- [57] Flavio de Paula Santos, Elson de Campos, Marcelo Costa, Francisco Cristovao Lourenco Melo, Roberto Yzumi Honda, and Rogerio Pinto Mota, “Superficial modifications in TiO<sub>2</sub> and Al<sub>2</sub>O<sub>3</sub> ceramics”, Materials Research, vol. 6, pp. 353, (2003).

[58] Myung. M. Sung, G. Jonathan Kluth, and Roya Maboudian, “Formation of alkylsiloxane self-assembled monolayers on  $\text{Si}_3\text{N}_4$ ”, J. Vac. Sci. Technol. A, vol. 17(2), pp. 540, (1999).

